Desalination and Water Treatment
www.deswater.com
doi: 10.5004/dwt.2022.28419

258 (2022) 111–122
May

Degradation of a basic textile dye by inactivated calcium peroxide

Behzat Balci*, F. Elcin Erkurt, Fuat Budak, Zeynep Zaimoglu, Mesut Basibuyuk, H. Kivanc Yesiltas

Department of Environmental Engineering, Cukurova University, Balcali/Saricam, Adana 01136, Turkey, Tel. +905369246018; email: behzatbalci@gmail.com (B. Balci), Tel. +905073174347; email: eerkurt@cu.edu.tr (F. Elcin Erkurt), Tel. +905334312631; email: fbudak@cu.edu.tr (F. Budak), Tel. +905324133434; email: zeynepz@cu.edu.tr (Z. Zaimoglu), Tel. +905324020561; email: basibuyuk@cu.edu.tr (M. Basibuyuk), Tel. +905053557079; email: hkyesiltas@cu.edu.tr (H. Kivanc Yesiltas)

Received 21 December 2021; Accepted 20 March 2022

ABSTRACT

Calcium peroxide (CaO_2) is an environmentally friendly oxidant and can be used to decolorize textile wastewater. In this study, CaO_2 was used directly without any activator to degrade Basic blue 41 (BB41) from simulated textile wastewater (STW), including auxiliary production chemicals. The characterization of the synthesized CaO_2 was investigated by scanning electron microscopy, energy-dispersive X-ray, X-ray diffraction and Fourier-transform infrared spectroscopy analyses. The optimum pH was found to be 7 for the degradation of the BB41. Thermodynamic studies showed that the degradation of the BB41 by CaO_2 is endothermic and spontaneous. The activation energy for the oxidation reaction was found 52.954 kJ mol^{-1}. 0.4 g CaO_2 was found to be sufficient for the removal of BB41 with 99.6% removal efficiency. The experiments showed that the CaO_2 can effectively oxidize organic-based auxiliary chemicals in STW. Over 80% chemical oxygen demand removal efficiency from STW was obtained with 2.0 g CaO_2. The study results showed that CaO_2 can be used as an effective and environmentally friendly oxidant for the decolorization of the textile wastewater.

Keywords: Colored wastewater; Basic blue 41; Oxidation

1. Introduction

The textile industry produces large amounts of wastewater, including dyes, due to the dyeing of fabric in the dyeing unit. Since the dye is not entirely fixed on the fabric, about 10%–15% of the dye transfers to wastewater [1]. Discharge of the textile wastewater without treatment with an appropriate method causes the transfer of dyes to aquatic environments [2]. The presence of dyes in the water bodies have adverse effects on ecosystems, such as decreasing dissolved oxygen levels, lowering the gas transfers, reducing light penetration and toxicity to aquatic organisms [3]. Most dyes are recalcitrant to biodegradation due to their aromatic structures [4]. Different technologies are used to remove dye-containing wastewaters, such as membrane filtration, adsorption, and advanced oxidation processes [5–7]. Advanced oxidation processes (AOP) stand out among the dye removal processes due to the mineralization of the dye molecules to non-toxic products. Hydrogen peroxide (H_2O_2) based AOP such as Fenton and Fenton-like process are widely used to oxidize dye molecules. The use of catalysts such as UV, iron element and special metal complexes is required to oxidize dye molecules with Fenton and Fenton-like processes. The use of catalysts enhances the oxidation efficiency but increases the operating costs of the processes and reveals the potential for metal pollution. In addition, Fenton and Fenton-like processes are usually effective in a narrow acidic media [8–11]. H_2O_2 is a powerful oxidant that produces the hydroxyl radical ($^{\bullet}OH$). However, H_2O_2 is unstable and decomposes rapidly [12].

* Corresponding author.

CaO_2 is an innovative environment-friendly strong oxidant (E^0 = 2.01 V) and is also known as a solid form of H_2O_2. CaO_2 slowly releases O_2 and H_2O_2. Oxidizing radicals, $^{\bullet}OH$, $^{\bullet}HO_2$ and $^{\bullet}O_2$, are produced by the H_2O_2, which is released from the surface of CaO_2 [Eqs. (1)–(5)]. According to the stoichiometric equation, 1.0 g of CaO_2 can produce a maximum of 0.47 g of H_2O_2 [12,13]. CaO_2 has some advantages such as a long lifetime, easy transport, and high stability compared to H_2O_2 [14].

$$CaO_2 + 2H_2O \rightarrow H_2O_2 + Ca(OH)_2 \quad (1)$$

$$2H_2O_2 \rightarrow 2H_2O + O_2 \quad (2)$$

$$H_2O_2 + e^- \rightarrow {}^{\bullet}OH + OH^- \quad (3)$$

$$^{\bullet}OH + H_2O_2 \rightarrow H_2O + {}^{\bullet}HO_2 \quad (4)$$

$$^{\bullet}HO_2 \rightarrow {}^{\bullet}O_2 + H^+ \quad (5)$$

Some activators such as Fe^0, Fe^{+2}, Fe^{3+} are used to enhance the production of oxidizing radicals released from CaO_2 [12,13,15,16]. However, iron pollution potential, disposal of the iron sludge, cost of catalysts are the disadvantages of using CaO_2 with activators. Calcium is an essential element for living organisms and CaO_2 has no toxic potential. CaO_2 is one of the safest metal oxides among other metal oxides. [17,18]. On the other hand, the use of a catalyst to enhance the oxidation capacity of CaO_2 undermines the CaO_2 process's potential to be environmentally friendly. The studies based on CaO_2 oxidation focus on the remediation of the polluted soils, groundwater, and activated sludge biomass [16,19–21]. The lack of studies on removing specific pollutants such as dyes from industrial wastewater with CaO_2 in the literature draws attention. Since CaO_2 is a strong and environmentally friendly oxidant, the potential of CaO_2 for the removal of specific pollutants from industrial wastewater should be investigated extensively.

Generally, distilled water was used as an aqueous phase in the studies based on removing textile dyes by AOP [7,10,22,23]. However, textile wastewater contains different salts and organic substances together with dyes. The complex structure of textile wastewater affects the removal of dyes in the oxidation processes. It is considered that the data obtained from working with a meticulously prepared simulated textile wastewater containing production chemicals is more suitable for evaluating the performance of oxidants in real-scale plants.

The study's objective is to investigate the potential use of CaO_2 without any activator to remove a textile dye Basic blue 41 (BB41) from simulated textile wastewater (STW) containing auxiliary production chemicals. Also, understanding the effects of some independent parameters such as pH, CaO_2 dosage and temperature on the oxidation of the BB41 by CaO_2 were aimed. Using directly inactivated CaO_2 in the oxidation process without metal or metal complex activators is an environmentally friendly approach as it will not cause metal pollution.

2. Material and methods

2.1. Characterization of the CaO_2

Scanning electron microscopy (SEM) (FEI, Quanta 650 Field Emission SEM, USA) was used to investigate the surface morphology of the synthesized CaO_2 with 5,000 and 10,000x magnification. The elemental analysis of the CaO_2 was determined by energy-dispersive X-ray (EDX) analysis (FEI, Quanta 650 Field Emission SEM, USA). Identification of the crystalline structure of CaO_2 was carried out by X-ray diffraction (XRD) analysis in 2θ scan range of 10°–90° (PANalytical Empyrean XRD, UK). Fourier-transform infrared spectroscopy (FTIR) (Jasco, FT/IR-6700, USA) was used in the range of to investigate associated functional groups of CaO_2. FTIR spectrum is recorded between 4,000 and 400 cm^{-1}.

2.2. Synthesis of CaO_2

In this study, the synthesis of the CaO_2 particles was carried out by precipitation with H_2O_2 at alkaline conditions. 8 g of calcium chloride (Merck, 99.5%, $CaCl_2{\cdot}2H_2O$) was dissolved in 40 mL deionized water. 120 mL polyethylene glycol (Merck, PEG200) was added to the solution as a surface modifier. 25 mL of 35% H_2O_2 (Merck) was added at 1 mL min^{-1} to the solution and mixed for 30 min at 20°C. Then 60 mL (1 N) KOH (Merck) was added to the solution to obtain the precipitate. The final volume of the mixture was adjusted to 200 mL by deionized water. The mixture was stirred within 2 h at 20°C to obtain a yellowish solution. The mixture was centrifuged to separate the solid phase. The solid phase was washed with distilled water several times to remove the KOH residuals and dried at 70°C for 24 h.

2.3. BB41 oxidation experiments

BB41 oxidation studies were carried out with STW. The composition of the STW was determined according to the process of a textile facility located in Adana/Turkey. The auxiliary chemicals used in production stages were obtained from the facility. The concentrations of the auxiliary chemicals in STW were determined according to the amount of usage dosage in production stages and dilution factor from production to wastewater generation in the facility. The STW composition is given in Table 1.

BB41 oxidation studies were performed as batch experiments with 200 mL STW at 300 rpm in a temperature controlled orbital shaker. The effect of pH (4–9), CaO_2 dosage (0.1–0.5 g) and temperature (5°C–30°C) were studied onto oxidation of a constant 200 mg L^{-1} BB41 concentration. Chemical oxygen demand (COD) removal studies were performed with different dosages of CaO_2 (0.2–2.0 g). The reuse of CaO_2 after BB41 oxidation was investigated in 4 cycles. Control groups were performed without CaO_2 under the same conditions.

Table 1
Composition of the simulated textile wastewater

Production chemical	Description	Conc. in STW
BB41	Dye	200 mg L^{-1}
Modified starch	Sizing agent	1,000 mg L^{-1}
NaCl	Dyeing promoter	3,000 mg L^{-1}
$NaHCO_3$	Dyeing promoter, pH adjuster	1,500 mg L^{-1}
Acetic acid	pH adjuster	0.11 mL L^{-1}
%10 NaOH	Mercerization	0.57 mL L^{-1}
H_2O_2	Bleaching agent	0.18 mL L^{-1}
Stabilol ZM	Stabilizer	0.60 mL L^{-1}
Cottoclarin TR	Wetting agent	0.40 mL L^{-1}
Serawet CAS	Rapid wetting agent	0.20 mL L^{-1}
Perlavin SRD	Soaping agent	0.50 mL L^{-1}
Securon 1420	Complexing agent for dyeing	0.20 mL L^{-1}
Locanite CNT	Washing agent	60 mg L^{-1}
Seragal MIP-O_2	Dyeing auxiliary	125 mg L^{-1}
Serocon MLU	Dyeing auxiliary	50 mg L^{-1}
Colorfix NF2P	Dyeing auxiliary	50 mg L^{-1}
Setasil KF-1920	Softening agent	50 mg L^{-1}
Tubingal MAC	Sanforizing auxiliary	125 mg L^{-1}
Belsoft 200	Softening agent	50 mg L^{-1}
COD		2,050 mg L^{-1}
Conductivity		11,455 μs cm^{-1}
pH		8.05

Table 2
Constants of pseudo-first-order model for different temperatures

Temperature, °C	k_{obs}, min^{-1}	R^2
5	0.0161	0.985
10	0.0262	0.989
15	0.0422	0.991
20	0.0611	0.990
25	0.0817	0.992
30	0.105	0.991

2.4. Analytical methods

Analysis of residual dye concentrations were performed with a calibration curve prepared at 609 nm (Perkin Elmer Lambda 35 UV/VIS, USA, spectrophotometer). The COD analyses of the samples were conducted by Closed Reflux Method (Standard Methods, 5220 C).

2.5. Statistical analysis

All dye degradation experiments were carried out in triplicate. The statistical evaluations of the data obtained from dye oxidation experiments were conducted by SPSS Statistics 20.0 with a confidence interval of 95% ($p \leq 0.05$).

3. Results and discussion

3.1. Characterization of the CaO_2

The SEM analysis showed that the CaO_2 particles generally have irregular shapes and different congregate structures (Fig. 1). The agglomeration of the CaO_2 particles is caused by the high surface energy of the CaO_2 [24]. The Oxygen and Calcium weight percent of the synthesized CaO_2 was determined as 52.76% and 43.45%, respectively, by analysis of EDX (Fig. 2). The carbon weight percent was determined as 3.79%, which belongs to the PEG200 surface stabilizer. The untitled peaks belong to Au element, which was used as a coating material before the EDX analysis.

The dominant peaks (2θ = 29.2°, 30.0°, 35.6°, 47.2°, 51.2°, 52.7°, 60.6°, 62.3°, 73.9°, 75.4°, 76.6°, 82.8°, 83.2°, 84°, 8°, 86.3°) obtained from the XRD analysis strongly matched with the molecule of CaO_2 (Reference code: 98-061-9462) (Fig. 3). The XRD patterns confirmed the tetragonal structure of CaO_2 [24,25].

The FTIR analyses were carried out for BB41, CaO_2 before and after degradation experiments. The peaks that appeared at the 3,337; 2,922 and 1,605 cm^{-1} for the FTIR of BB41 are related to –OH, $–CH_3$, –N=N– stretching (Fig. 4a). The peaks appeared between 1,000–1300 cm^{-1} and 400–800 cm^{-1} bands correspond to –S=O– vibration and aromatic rings of the BB41, respectively. [26]. The broad weak signal appeared at 3,000–3,600 cm^{-1} in the FTIR spectrum of the unused CaO_2 belongs to the –OH bond stretching due to adsorption of water molecules onto CaO_2

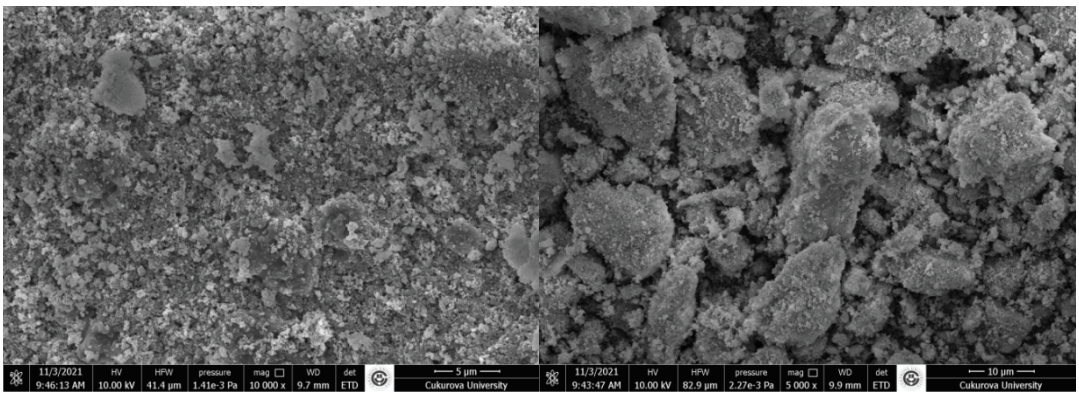

Fig. 1. SEM images of CaO_2.

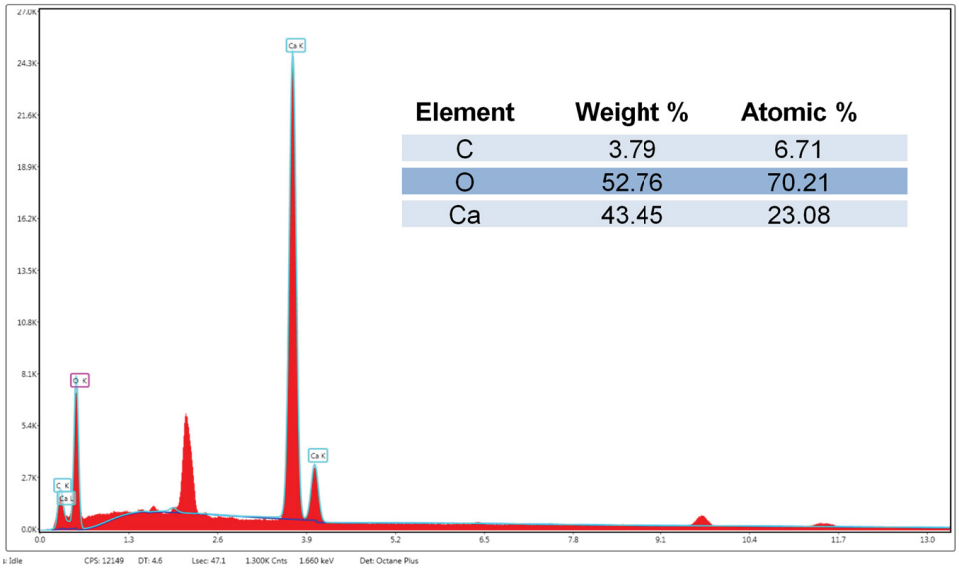

Fig. 2. EDX of CaO_2.

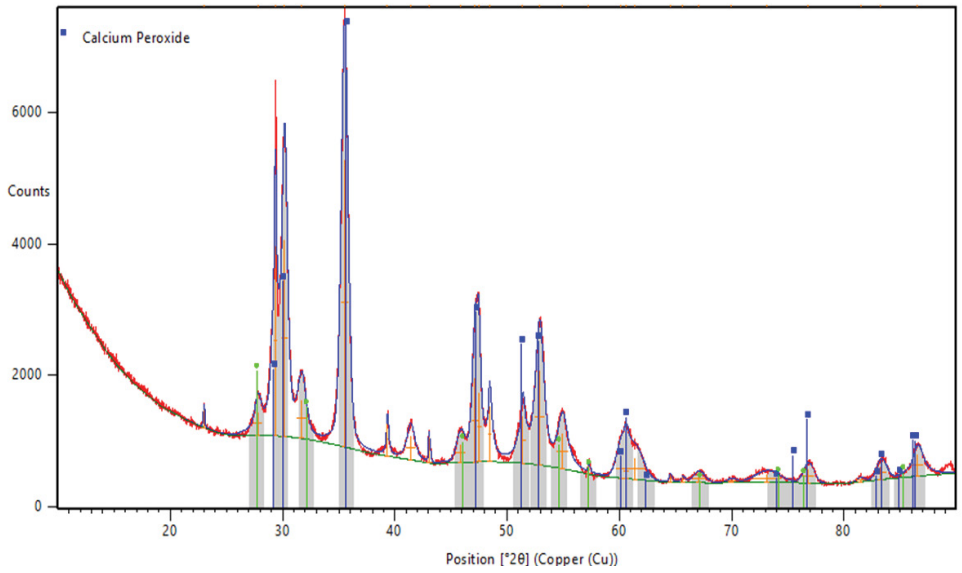

Fig. 3. XRD analysis of CaO_2.

(Fig. 4b). The typical signal detected between 1,200 and 1,400 cm^{-1} is related to the bending vibration of O–Ca–O [27,28]. The signal appeared at 871 cm^{-1} belongs to O–O stretching vibration of peroxide [27,29]. The peak detected 2,900–2,990 cm^{-1} band related to C–H stretching belongs to the surface stabilizer PEG200 [30]. It was found that the density of the peaks correspond to O–Ca–O bending vibration and O–O stretching decreased after the oxidation experiments due to consumption of CaO_2 during the degradation of the BB41 (Fig. 4c). The signals belonging to the BB41, such as $–CH_3$, –N=N– and –S=O– were not detected in the FTIR analysis of CaO_2 after the BB41 degradation. The FTIR analysis showed that the surface of CaO_2 did not contain BB41 molecules after the oxidation process. The BB41 molecules may be degraded in the liquid phase and on the surface of CaO_2. The main removal mechanism of BB41 by CaO_2 is the oxidation process.

3.2. BB41 oxidation experiments

3.2.1. Effect of pH on degradation of BB41 by CaO_2

H_2O_2 based oxidation processes are greatly affected by the pH of the solution [31]. The effects of four different pH values (4, 5, 6, 7, 8 and 9) on the degradation of 200 mg L^{-1} by 0.5 g CaO_2 were carried out at 20°C (Fig. 5). It was found that the pH had a significant effect on the oxidation of the BB41 by CaO_2 ($p < 0.05$). The experiments

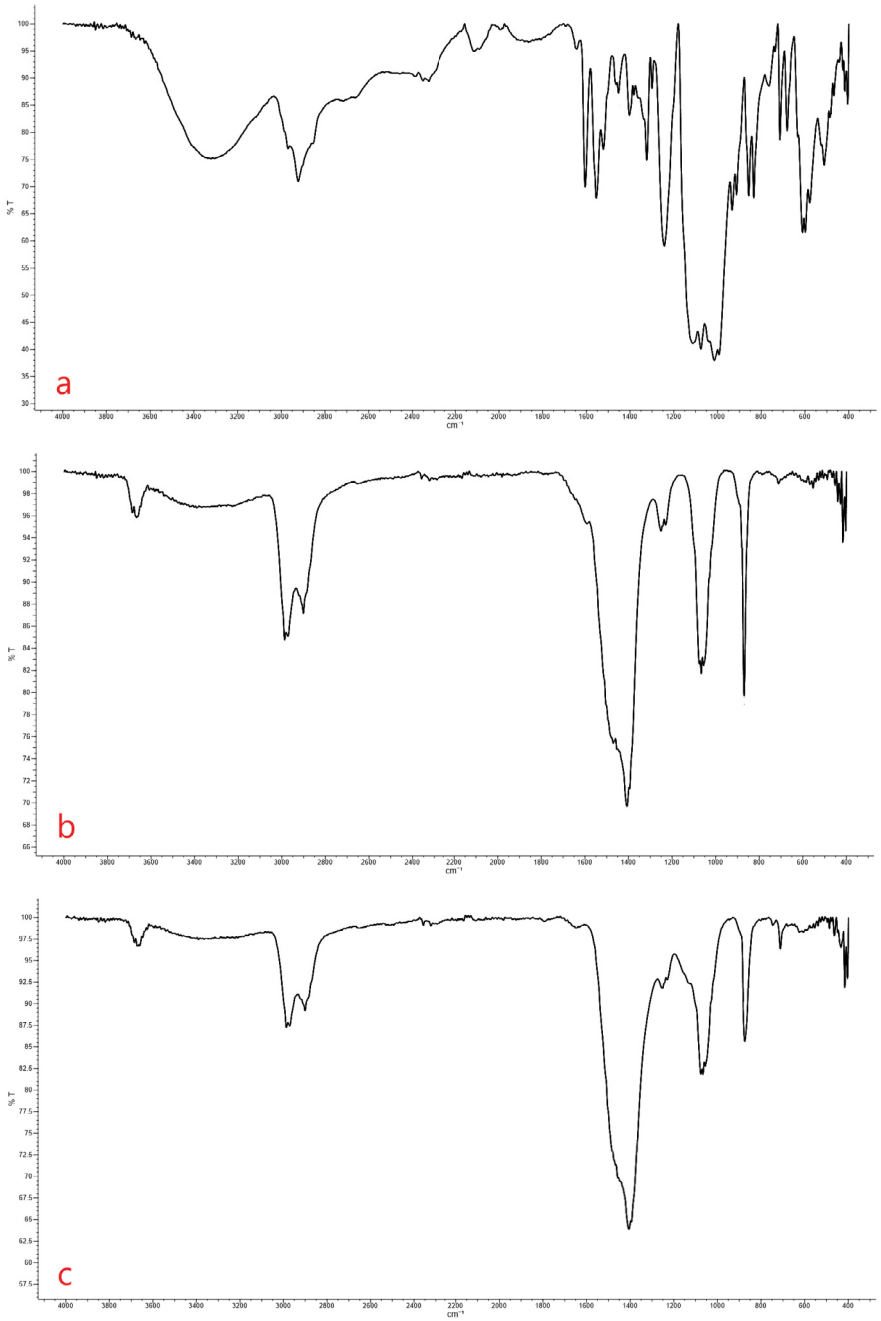

Fig. 4. FTIR for BB41 (a), unused CaO_2 (b) and used CaO_2 (c).

showed that the degradation efficiency of BB41 significantly decreased below pH 6. The low degradation efficiency at acidic pH can be explained by the increase of CaO_2 solubility and decreasing H_2O_2 production due to the reaction of excessive H^+ ions with CaO_2 directly [32,33]. While the degradation efficiency reached over 99.5% within 60 min for pH 7, it reached over 99.5% within 150 and 180 min for pH 8 and 9, respectively. The peroxide ions (O_2^{-2}) released from CaO_2 react with H^+ ions produced from water molecules to form H_2O_2. OH^- ions can neutralize H^+ ions at alkaline conditions. The oxygen production increases and the H_2O_2 production decreases with increasing pH. Therefore oxidation rate decreased in high pH levels due to decreasing H_2O_2 production by CaO_2 [33–35]. Further experiments were performed at pH 7.

3.2.2. *Effect CaO_2 dosage on the degradation of BB41*

Determining the optimum oxidant dosage is an important parameter for operating real-scale applications under optimum conditions. The influence of the CaO_2 dosage (0.1, 0.2, 0.3, 1.0, 0.4, 0.5 g) on the oxidation process was performed with 200 mg L^{-1} BB41 at 20°C. It determined that

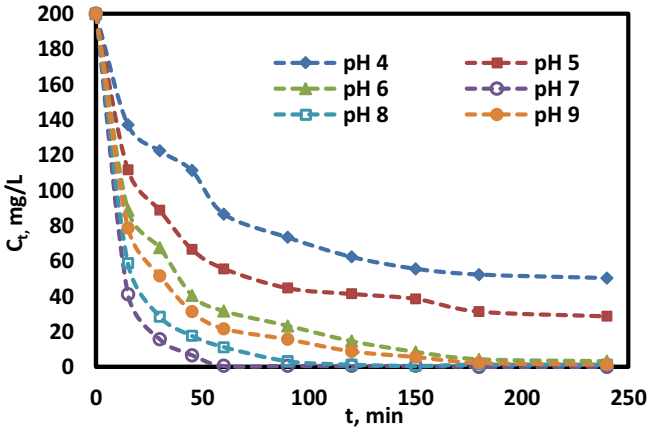

Fig. 5. Effect of pH on degradation of the BB41.

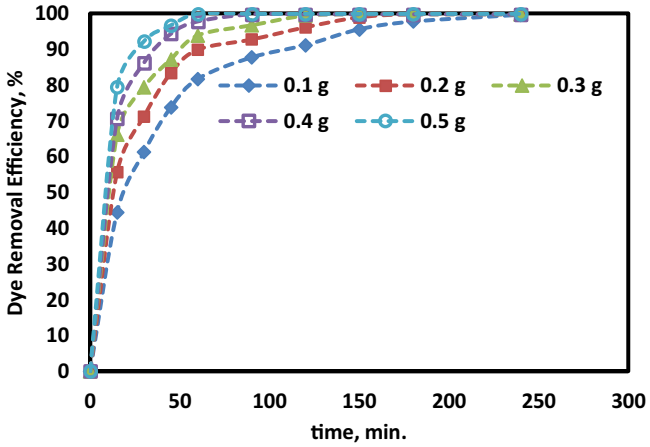

Fig. 6. Effect of CaO_2 dosage the degradation of the BB41.

the CaO_2 dosage had a significant effect on the oxidation of the BB41 by CaO_2 ($p < 0.05$). Over 99% BB41 decolorization was obtained for all CaO_2 dosages at different times (Fig. 6). The times to reach decolorization of BB41 efficiencies above 99% for 0.1 and 0.5 g CaO_2 were determined 240 and 60 min, respectively. The BB41 removal efficiency was calculated as 99.75% within 90 min for 0.4 g CaO_2 dosage. High BB41 degradation efficiencies at high amounts of CaO_2 can be explained by the increasing oxidizing radicals released from CaO_2 [36]. Large volumes of tanks with high contact time will be needed to achieve dye removal efficiencies of over 99% for doses below 0.4 g in possible real-scale applications. While this situation provides an advantage in operating costs due to low oxidant dosages, it will cause an increase in investment costs for large volume tanks requirement. 0.4 g CaO_2 was found to be sufficient to remove BB41 under optimum conditions. Further experiments were performed with 0.4 g CaO_2 dosage.

3.2.3. Effect of temperature on the degradation of BB41

Temperature plays an important role and can alter the efficiency of oxidation processes. Influence of temperature (5°C, 10°C, 15°C, 20°C, 25°C and 30°C) on the

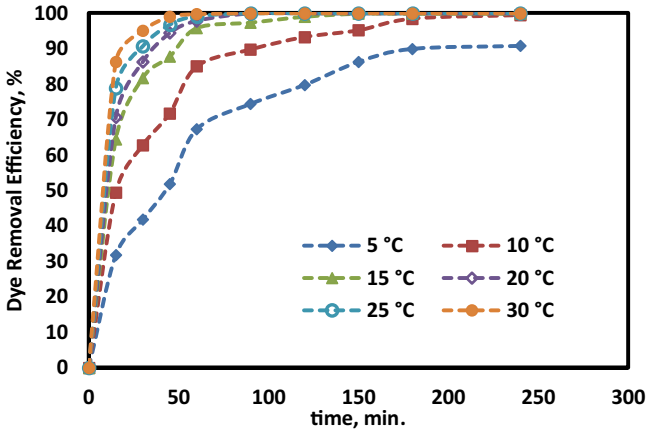

Fig. 7. Effect of temperature on the degradation of the BB41.

degradation of BB41 was carried out with 0.4 g CaO_2 for 200 mg L^{-1} dye concentration. It was found that the temperature of the STW had a significant effect on the oxidation of the BB41 by CaO_2 ($p < 0.05$). It can be seen from Fig. 7 increasing the temperature has a positive impact on the degradation of the BB41. The BB41 degradation efficiency within 60 min for 5°C, 10°C, 15°C, 20°C, 25°C and 30°C was found to be 67.2%, 84.6%, 95.7%, 98.11%, 99.15% and 99.6%, respectively. High dye removal efficiencies at higher temperatures can be explained by the increase in the decomposition of the H_2O_2 with increasing temperature. Thus, more oxidizing radicals are released by H_2O_2. Also, high temperatures give more energy to reactants to overcome the activation energy [37].

3.2.4. Kinetics and thermodynamics of the BB41 degradation by CaO_2

Linear form of pseudo-first-order reaction model was used to determine the degradation rates of 200 mg L^{-1} BB41 with 0.4 g CaO_2 for different temperatures [Eq. (6)].

$$\ln\left(\frac{C_t}{C_0}\right) = -k_{obs}t \tag{6}$$

where C_t is the residual dye concentration (mg L^{-1}), C_0 is the initial dye concentration (mg L^{-1}), k_{obs} (min^{-1}) is the rate constant of pseudo-first-order model and t is time (min.). k_{obs} can be calculated from the plot of $\ln(C_t/C_0)$ vs. t (figure not shown here) [38]. The R^2 values obtained from the pseudo-first-order kinetic model analysis ranged from 0.985 to 0.991. High R^2 values showed that the data fit pseudo-first-order kinetic models well. Many studies reported that the degradation kinetics of the textile dye based on H_2O_2 is described by the pseudo-first-order model [39–42]. It was found that the k_{obs} value increased with increasing temperature. Increasing in rate constants with rising temperature can be explained by the increase in molecular collision frequency with increasing temperature [43]. The maximum k_{obs} (0.105 min^{-1}) were obtained at 30°C. High rate constant values showed that the mineralization of the BB41 occurred within a short time.

The reaction's activation energy (E_a) is a crucial parameter for H_2O_2 based oxidation processes to understand how fast the reaction is completed. The linear form of the Arrhenius equation [Eq. (7)] was used to calculate the activation energy [44].

$$\ln k = \ln A - \frac{E_a}{RT} \tag{7}$$

where A is the frequency factor, E_a is the activation energy (kJ mol^{-1}), R is the ideal gas constant (0.0083 kJ mol^{-1} K^{-1}), T is the absolute temperature (K) and k is the pseudo-first-order rate constant (min^{-1}). E_a can be calculated from the plot of ln$k$ vs. 1/T [45]. The thermodynamic parameters including standard free energy ($\Delta G°$), enthalpy ($\Delta H°$), and entropy ($\Delta S°$) were calculated using the following equations:

$$\Delta G° = -RT \ln K_C \tag{8}$$

The value of K_C can be calculated from Eq. (9).

$$K_C = \frac{C_D}{C_T} \tag{9}$$

where C_D is the amount of BB41 concentration at equilibrium time (mg L^{-1}), C_T is the BB41 residual concentration in liquid phase at equilibrium (mg L^{-1}). Van't Hoff equation was used to calculate the thermodynamic parameters (Fig. 8). $\Delta H°$, and entropy $\Delta S°$ can be obtained from the slope and intercept of the lnK_C vs. 1/T plot [Eq. (10)] [37].

$$\ln K_C = \frac{-\Delta H°}{RT} + \frac{\Delta S°}{R} \tag{10}$$

The E_a value was calculated as 52.954 kJ mol^{-1} with a 0.9883 R^2 value (Fig. 9). The activation energy for the degradation of the BB41 by CaO_2 is greater than the diffusion-controlled (~29 kJ mol^{-1}) reaction. It is thought to be the rate-limiting step of the BB41 oxidation by CaO_2 is a surface-chemical reaction [46,47]. The negative $\Delta G°$ values were obtained for all studied temperatures (Table 3). Negative $\Delta G°$ values showed that the degradation of BB41 by CaO_2 is spontaneous and the extent of the spontaneity increases with increasing the temperature. The positive value of $\Delta H°$ indicates the endothermic nature of the BB41 degradation by CaO_2. A positive value of $\Delta S°$ (0.498 J mol^{-1} K^{-1}) indicates to the increase the randomness in the degradation of the BB41 by CaO_2 [9].

3.3. Reuse of CaO_2

Investigating the reuse potential of an oxidant is an essential step towards reducing operating costs on an industrial scale. Four cycles were performed for the investigation of the reusability of CaO_2. The experiments on reuse of CaO_2 were performed with 200 mg L^{-1} BB41 and 0.4 g CaO_2 at 20°C. Before the cycles, the CaO_2 particles

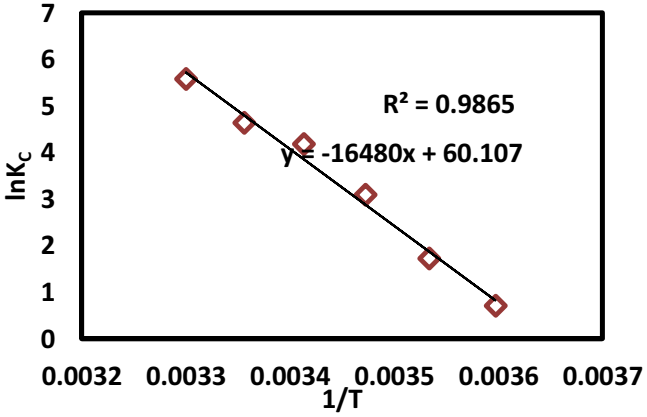

Fig. 8. Van't Hoff plot.

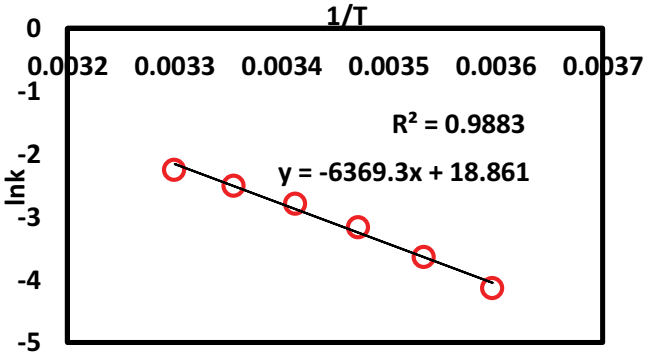

Fig. 9. Arrhenius plot.

Table 3
Thermodynamic parameters

Temperature, °C	E_a, kJ mol^{-1}	$\Delta G°$, kJ mol^{-1}	$\Delta H°$, J mol^{-1}	$\Delta S°$, J mol^{-1} K^{-1}
5	52.954	–1.662	1.367	0.498
10		–4.060		
15		–7.425		
20		–10.188		
25		–11.507		
30		–14.055		

were separated by centrifuging then added to fresh STW. The BB41 degradation efficiencies within 90 min by CaO_2 for 1st, 2nd, 3rd and 4th cycle were determined as 99.75%, 92.5%, 79.4% and 57.2%, respectively (Fig. 10). It was found that the BB41 degradation efficiencies are at acceptable levels within 3rd cycle. On the other hand, decolorization efficiency dramatically decreased in 4th cycle due to consumption of oxidizing radicals produced by CaO_2.

3.4. COD removal from STW by CaO_2

The specific COD sources of textile wastewater are modified starch, dyes and organic-based other auxiliary chemicals. COD removal experiments from STW by CaO_2 were carried out to understand the oxidation potential of CaO_2 for BB41 and the other organic molecules. The experiments were performed with STW containing 200 mg L^{-1} BB41 and different CaO_2 dosages (0.2, 0.4, 0.8 1.0, 1.5 and 2.0 g). COD removal efficiencies with different amounts of CaO_2 were evaluated for three different reaction times (240, 360 and 480 min.). The initial COD value of STW containing 200 mg L^{-1} BB41 was calculated as 2,180 mg L^{-1}. The COD value of separate 200 mg L^{-1} BB41 in distilled water was determined as 292 mg L^{-1}. Modified starch and organic-based auxiliary chemicals are the other COD sources of the STW. It was found that the COD removal efficiency increased with increasing CaO_2 dosage ($p < 0.05$) (Fig. 11). COD removal efficiency with 0.2 and 2.0 g CaO_2 for 480 min were determined 46.58% and 80.73%, respectively. While the BB41 was completely removed by 0.4 CaO_2 within 240 min, the COD removal efficiency was found to be 35.1%. For an effective COD removal, a CaO_2 dose of over 0.8 g and a reaction time of over 360 min are required. The COD removal experiments showed that the CaO_2 oxides BB41 molecules along with organic-based substances in STW.

An extensive literature review including experimental variables was conducted on the degradation of the BB41 by H_2O_2-based oxidation processes (Table 4). Duc [48] and Solomon et al. [49] used the Fenton process with Fe^{2+} catalyst and reported over 97% BB41 decolorization efficiencies. While Duc [48] reported 120 min to reach equilibrium with 0.025 g L^{-1} Fe^{2+} and 386 mg L^{-1} H_2O_2 concentrations, Solomon et al. [49] reported the equilibrium time as 60 min with 0.6 g L^{-1} Fe^{2+} and 1,055 mg L^{-1} H_2O_2. It is seen that high doses of chemicals are needed to reach high BB41 removal efficiency in a shorter time. High reaction times with low chemical doses will require large tank volumes in real-scale applications. On the other hand, high iron concentrations cause high amounts of sludge. The pH parameter is crucial in the Fenton process. Generally, an acidic medium is required to generate oxidizing radicals by the reaction of H_2O_2 with Fe ions [66]. pH adjustment in large amounts of wastewater volumes causes an increase in operating costs. Also, the final neutralization of the wastewater may produce large amounts of iron-containing sludge, contributing to metal pollution [67]. It can be seen from Table 4 studies on BB41 degradation have focused on photocatalytic processes. Some independent parameters such as initial dye concentration, irritation intensity and type, catalyst dose, and type significantly affect the degradation of textile dyes by photocatalytic processes [68]. Researchers other than Kartiko et al. [57] and Rapsomanikis et al. [58] used low concentrations of BB41 in catalytic processes. Initial dye concentration is an important parameter that affects the removal rates. Removing pollutants in high concentrations requires large catalytic doses or irritation times [69]. High operational cost due to UV irradiation is the main disadvantage of the photocatalytic processes. Energy efficiency for converting photons to oxidizing radicals ranges between 0.0002%–5%. Therefore efficient catalysts are required to enhance the efficiency of the process [70]. Titanium dioxide (TiO_2) is widely used in photocatalytic processes due to its photoactivity, stability, optical and electronic properties [69]. On the other hand, many studies reported the toxic effects of nano-TiO_2 on aquatic organisms and mammals [71–74]. Over 20 mg L^{-1} TiO_2 exhibits significant toxic effects on ovarian cells of *Bombyx mori* [75]. The potential toxic effects of TiO_2 on living organisms

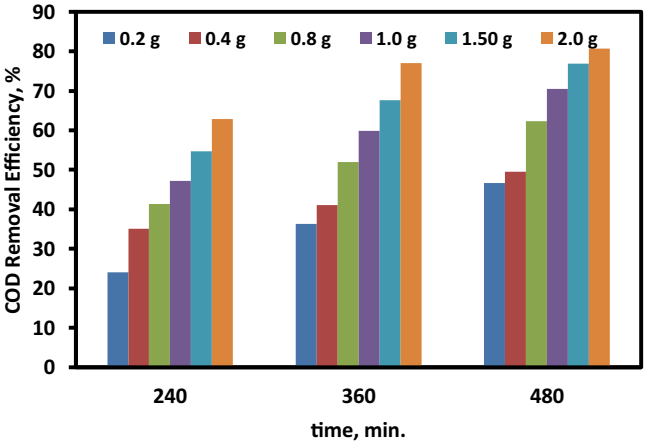

Fig. 11. Removal COD from STW by CaO_2.

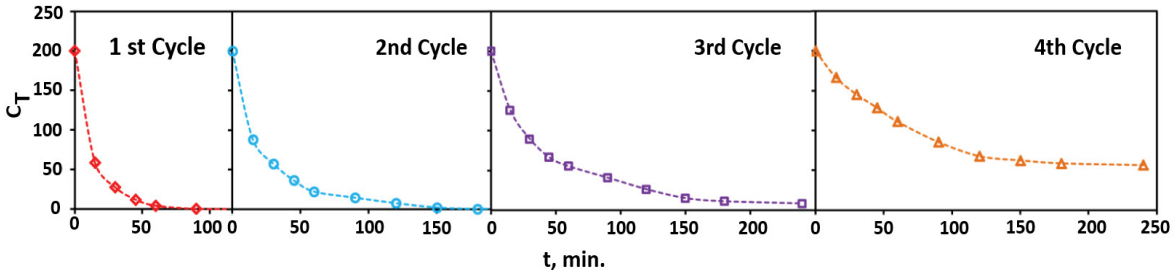

Fig. 10. Reuse of CaO_2 for BB41 degradation.

Table 4
Comparison of H_2O_2-based oxidation processes for the degradation of the BB41

Oxidation process	Catalyst	BB41 conc.	Aqueous phase	Catalyst dose, g L^{-1}	UV	H_2O_2 dose, mg L^{-1}	pH	Time, min	Dye removal, %	Reference
Fenton	Fe^{2+}	200 mg L^{-1}	Distilled water	0.025	–	386	3.2	120	97.8	[48]
Fenton	Fe^{2+}	135 mg L^{-1}	Distilled water	0.60	–	1,055	<7	60	97.2	[48,49]
Photocatalytic	MIL-100 (Fe) (Metal–organic framework)	20 mg L^{-1}	Distilled water	0.040	UV-C	–	5	90	>99	[50]
Photocatalytic	Palygorskite/TiO_2 film reactor	12 mg L^{-1}	Distilled water	–	UV-A	–	6.5	90	>99	[51]
Photocatalytic	TiO_2-ZnO	20 mg L^{-1}	Distilled water	10	Solar radiation	–	6.21	60	99.16	[52]
Photocatalytic	$CoCr_2O_4$	10 mg L^{-1}	Distilled water	0.50	Visible light	–	9	180	95	[53]
Photocatalytic	Activated carbon/TiO_2	54.8 Pt.Co	Distilled water	5.2	UV-C	–	6	45	96	[54]
Photocatalytic	TiO_2 film reactor	25 mg L^{-1}	Distilled water	–	UV-C	–	7	100	98.7	[55]
Photocatalytic	TiO_2/calcium alginate	30 mg L^{-1}	Distilled water	0.10	Solar radiation	–	7	180	~96	[56]
Photocatalytic	TiO_2-Fe_3O_4-bentonite film reactor	200 mg L^{-1}	Distilled water	–	Mercury lamp	–	5.5	161	42.26	[57]
Photocatalytic	Halloysite/TiO_2 film reactor	120 mg L^{-1}	Distilled water	–	UV-C	–	Natural	140	~99	[58]
Photocatalytic	Zn:SnO_2/Al_2O_3 NT	20 mg L^{-1}	Distilled water	0.50	Visible light	–	Natural	100	98.2	[59]
Photocatalytic	Fe_2O_3/TiO_2	10 mg L^{-1}	Distilled water	–	Visible light		Natural	240	97.54	[60]
Photocatalytic	Pyritic coal	20 mg L^{-1}	Distilled water	1.0	Solar radiation		6	180	99.5	[61]
Photocatalytic	ZnO	20 mg L^{-1}	Distilled water	0.020	UV-C		4	180	72.36	[62]
Photocatalytic	$CaFe_2O_4$ film reactor	20 mg L^{-1}	Distilled water	–	Solar radiation	–	~6.4	180	85	[63]
Sonochemical	TiO_2	15 mg L^{-1}	Distilled water	1,000	–	250	8	180	89.5	[64]
Sonochemical	TiO_2	30 mg L^{-1}	Distilled water	0.20	–	250	8.5	180	82.2	[65].
Separate CaO_2 (2.0 g L^{-1})	–	200 mg L^{-1}	STW	–	–	–	7.0	60	99.6	This study

raise doubts about the environmental friendliness of using this catalyst in the photocatalytic wastewater treatment processes. The liquid phase of the studies given in Table 5 is distilled water. Doubtlessly using distilled water, including only dye molecules, is important to understand the specific interactions between dye molecules and oxidants. However, it is hard to understand the potential use of the oxidant in real applications by evaluating the results of these studies. We did not find a study using real textile wastewater or simulated textile wastewater in the H_2O_2-based oxidation of BB41 in the literature. The presence of anions such as Cl^- and HCO_3^- can cause the consumption of oxidizing radicals. $^{\bullet}Cl_2^-$ radical can be formed by the reaction of Cl^- with $^{\bullet}OH$ formed $^{\bullet}Cl_2^-$ which has less oxidation potential than the $^{\bullet}OH$. HCO_3^- causes $^{\bullet}OH$ consumption due to $^{\bullet}HCO_3$ formation [76]. In addition, the presence of organic substances, unlike the dye molecules, will cause the consumption of oxidizing radicals, which causes a decrease in dye removal efficiencies. In this study, 99.6% BB41 removal efficiency from STW, including textile production auxiliary chemicals, was

obtained with direct use of CaO_2. It can be seen from Table 4 BB41 oxidation studies were performed with different catalysts. On the other hand, the direct use of a metal oxide without any activator for the oxidation of the BB41 can be more cost-effective and environmentally friendly.

In the study, CaO_2 was used without any activator to remove the BB41 in the STW. CaO_2 releases H_2O_2 in an aqueous solution and H_2O_2 generates non-selective oxidizing radicals species such as $^{\bullet}OH$, $^{\bullet}HO_2$ and $^{\bullet}O_2$, which are responsible for the degradation of the BB41 molecules. The oxidation of the BB41 can be occurred in the STW and on the surface of the CaO_2. The FTIR analysis showed that the peaks belonging to the BB41 molecule were not detected in the FTIR analysis of CaO_2 after oxidation. The FTIR analysis showed that the BB41 molecules are not present on the surface of the CaO_2 after the oxidation process. It is thought to be the possible removal mechanism of BB41 from STW is oxidation as a result of the production of the oxidizing radicals by CaO_2.

4. Conclusion

In this study, CaO_2 was directly used to degrade BB41 from STW containing auxiliary textile production chemicals**.** The study results showed that the inactivated CaO_2 is an effective oxidant and can be directly used for the degradation of BB41. The use of CaO_2 without any activator can be an environmentally friendly process. The optimum pH was found to be 7 for the decolorization of the BB41. The experiments showed that the temperature has an important effect on the degradation of the BB41 by CaO_2. The oxidation of the BB41 is an endothermic reaction. 99.6% degradation efficiency was obtained with 0.4 g CaO_2 within 60 min. CaO_2 oxidizes BB41 along with the other organic-based substances in STW. It was found that 2.0 g CaO_2 is required to achieve COD removal efficiency over 80%.

Acknowledgement

The authors would like to thank to Cukurova University for their support.

References

[1] S.M. Lam, J.C. Sin, A.Z. Abdullah, A.R. Mohamed, Degradation of wastewaters containing organic dyes photocatalysed by zinc oxide: a review, Desal. Water Treat., 41 (2012) 131–169.
[2] W. Chairungsri, A. Subkomkaew, P. Kijjanapanich, Y. Chimupala, Direct dye wastewater photocatalysis using immobilized titanium dioxide on fixed substrate, Chemosphere, 286 (2022) 131762, doi: 10.1016/j.chemosphere.2021.131762.
[3] N. Oke, S. Mohan, Development of nanoporous textile sludge based adsorbent for the dye removal from industrial textile effluent, J. Hazard. Mater., 422 (2022) 126864, doi: 10.1016/j.jhazmat.2021.126864.
[4] T.C. Bessy, M.R. Bindhu, J. Johnson, S.M. Chen, T.W. Chen, K.S. Almaary, UV light assisted photocatalytic degradation of textile wastewater by $Mg_{0.8-x}Zn_xFe_2O_4$ synthesized by combustion method and in-vitro antimicrobial activities, Environ. Res., 204 (2022) 111917, doi: 10.1016/j.envres.2021.111917.
[5] S. Arefi-Oskoui, A. Khataee, S.J. Behrouz, V. Vatanpour, S.H. Gharamaleki, Y. Orooji, M. Safarpour, Development of MoS_2/O-MWCNTs/PES blended membrane for efficient removal of dyes, antibiotic, and protein, Sep. Purif. Technol., 280 (2022) 119822, doi: 10.1016/j.seppur.2021.119822.
[6] A. Mohmouda, F. Koolic, Y. Liud, Waste of pine seeds as bio-removal agent for methylene blue from aqueous solution: regeneration and single-stage batch design, Desal. Water Treat., 204 (2020) 144–154.
[7] S.B. Seror, D. Shamir, Y. Albo, H. Kornweitz, A. Burg, Elucidation of a mechanism for the heterogeneous electro-Fenton process and its application in the green treatment of azo dyes, Chemosphere, 286 (2022) 131832, doi: 10.1016/j.chemosphere.2021.131832.
[8] P. Neha, K. Vijyendra, G. Prabir, Degradation of 4-nitrophenol (4-NP) using Fe-loaded fly ash brick clay as a heterogeneous Fenton catalyst, Desal. Water Treat., 95 (2017) 170–179.
[9] Y. Zhu, Q. Xie, R. Zhu, Y. Lv, Y. Xi, J. Zhu, J. Fan, Hydrothermal carbons/ferrihydrite heterogeneous Fenton catalysts with low H_2O_2 consumption and the effect of graphitization degrees, Chemosphere, 287 (2022) 131933, doi: 10.1016/j.chemosphere.2021.131933.
[10] C. Liu, B. Yang, J. Chen, F. Jia, S. Song, Synergetic degradation of Methylene blue through photocatalysis and Fenton reaction on two-dimensional molybdenite-Fe, J. Environ. Sci., 111 (2022) 11–23.
[11] N. Hajipour, M. Ghorbanpour, A. Feizi, Application of photo-Fenton dye removal with γ-Fe_2O_3/bentonite nanocomposites prepared by solid-state reaction in wastewater treatment, Desal. Water Treat., 233 (2021) 311–318.
[12] C. Hou, J. Zhao, Y. Zhang, Y. Qian, J. Chen, M. Yang, X. Zhou, Enhanced simultaneous removal of cadmium, lead, and acetochlor in hyporheic zones with calcium peroxide coupled with zero-valent iron: mechanisms and application, Chem. Eng. J., 427 (2022) 130900, doi: 10.1016/j.cej.2021.130900.
[13] Z. Chen, M. Chen, K.Y. Koh, W. Neo, C.N. Ong, J.P. Chen, An optimized CaO_2-functionalized alginate bead for simultaneous and efficient removal of phosphorous and harmful cyanobacteria, Sci. Total Environ., 806 (2022) 150382, doi: 10.1016/j.scitotenv.2021.150382.
[14] M. Chen, Z. Chen, P. Wu, J.P. Chen, Simultaneous oxidation and removal of arsenite by Fe(III)/CaO_2 Fenton-like technology, Water Res., 201 (2021) 117312, doi: 10.1016/j.watres.2021.117312.
[15] R. Yang, G. Zeng, Z. Xu, Z. Zhou, J. Huang, R. Fu, S. Lyu, Comparison of naphthalene removal performance using H_2O_2, sodium percarbonate and calcium peroxide oxidants activated by ferrous ions and degradation mechanism, Chemosphere, 283 (2021) 131209, doi: 10.1016/j.chemosphere.2021.131209.
[16] J. Wang, X. Zhang, X. Zhou, M.G. Waigi, F.O. Gudda, C. Zhang, W. Ling, Promoted oxidation of polycyclic aromatic hydrocarbons in soils by dual persulfate/calcium peroxide system, Sci. Total Environ., 758 (2021) 143680, doi: 10.1016/j.scitotenv.2020.143680.
[17] D. He, B. Bao, M. Sun, J. Chen, H. Luo, J. Li, Enhanced dewatering of activated sludge by acid assisted heat–CaO_2 treatment: simultaneously removing heavy metals and mitigating antibiotic resistance genes, J. Hazard. Mater., 418 (2021) 126248, doi: 10.1016/j.jhazmat.2021.126248.
[18] X. Qiuxiang, H. Qi-Su, W. We, S. Jin, D. Xiaoh, N. Bing-Ji, Improving the treatment of waste activated sludge using calcium peroxide, Water Res., 187 (2020) 116440, doi: 10.1016/j.watres.2020.116440.
[19] J. Wang, Y. Lou, K. Feng, H. Zhou, B. Liu, G. Xie, D. Xing, Enhancing the decomposition of extracellular polymeric substances and the recovery of short-chain fatty acids from waste activated sludge: analysis of the performance and mechanism of co-treatment by free nitrous acid and calcium peroxide, J. Hazard. Mater., 423 (2022) 127022, doi: 10.1016/j.jhazmat.2021.127022.
[20] J.G. Kim, H.B. Kim, W.G. Jeong, K. Baek, Enhanced-oxidation of sulfanilamide in groundwater using combination of calcium peroxide and pyrite, J. Hazard. Mater., 419 (2021) 126514, doi: 10.1016/j.jhazmat.2021.126514.
[21] G. Zhang, Y. Shi, W. Chen, M. Dou, Z. Zhao, X. Wang, T. Zhang, Methane production from waste activated sludge by combining calcium peroxide pretreatment with zero valent iron bio-enhancement: performance and mechanisms, J. Cleaner Prod., 320 (2021) 128773, doi: 10.1016/j.jclepro.2021.128773.

[22] M.A.P. Cechinel, T.O. Guidolin, A.R. Silveira, T.J. Santos, O.R.K. Montedo, S. Arcaro, Coal mining pyritic waste in Fenton-like processes: raw and purified catalysts in Reactive blue 21 dye discoloration, Sci. Total Environ., 807 (2022) 150823, doi: 10.1016/j.scitotenv.2021.150823.
[23] T. Hussain, M. Hussain, S. Hussain, M. Kaseem, Microwave-assisted synthesis of $NiTe_2$ photocatalyst as a facile and scalable approach for energy-efficient photocatalysis and detoxification of harmful organic dyes, Sep. Purif. Technol., 282 (2021) 120025, doi: 10.1016/j.seppur.2021.120025.
[24] S. Zhang, Y. Wei, J. Metz, S. He, P.J. Alvarez, M. Long, Persistent free radicals in biochar enhance superoxide-mediated Fe(III)/Fe(II) cycling and the efficacy of CaO_2 Fenton-like treatment, J. Hazard. Mater., 421 (2022) 126805, doi: 10.1016/j.jhazmat.2021.126805.
[25] Y. Yin, T. Jiang, Y. Hao, J. Zhang, W. Li, Y. Hao, W. He, Y. Song, Q. Feng, W. Ma, Cascade catalytic nanoplatform based on ions interference strategy for calcium overload therapy and ferroptosis, Int. J. Pharm., 606 (2021) 120937, doi: doi: 10.1016/j.ijpharm.2021.120937.
[26] A.A. Alshehri, M.A. Malik, Biogenic fabrication of ZnO nanoparticles using *Trigonella foenum-graecum* (Fenugreek) for proficient photocatalytic degradation of methylene blue under UV irradiation, J. Mater. Sci.: Mater. Electron., 30 (2019) 16156–16173.
[27] K. Sajedeh, K. Akbar, B. Shahin, Fabrication of amine-decorated nonspherical microparticles with calcium peroxide cargo for controlled release of oxygen, J. Biomed. Mater. Res. A, 108 (2020) 136–147.
[28] A. Meesam, F. Usman, L. Shuguang, S. Yong, L. Ming, A. Ayyaz, S. Ali, A. Zain, Synthesis of controlled release calcium peroxide nanoparticles (CR-nCPs): characterizations, H_2O_2 liberate performances and pollutant degradation efficiency, Sep. Purif. Technol., 241 (2020) 116729, doi: 10.1016/j.seppur.2020.116729.
[29] L. Andrews, G.V. Chertihin, C.A. Thompson, J. Dillon, S. Byrne, C.W. Bauschlicher, infrared spectra and quantum chemical calculations of group $2MO_2$, O_2MO_2, and related molecules, J. Phys. Chem., 100 (1996) 10088–10099.
[30] E. Pramono, S.B. Utomo, V. Wulandari, F. Clegg, FTIR studies on the effect of concentration of polyethylene glycol on polimerization of Shellac, J. Phys. Conf. Ser., 776 (2016) 012053, doi: 10.1088/1742-6596/776/1/012053.
[31] Y. Tian, W. Fu, Q. Wang, Y. Tang, M. Zhou, High electron transfer rate and efficiency on Fe^0 modified by sulfidation and pre-magnetization for carbamazepine degradation by heterogeneous electro-Fenton in wide pH ranges, Chem. Eng. J., 427 (2022) 131694, doi: 10.1016/j.cej.2021.131694.
[32] P. Vijuksungsith, T. Satapanajaru, C. Chokejaroenrat, C. Jarusutthirak, C. Sakulthaew, A. Kambhu, R. Boonprasert, Remediating oxytetracycline-contaminated aquaculture water using nano calcium peroxide ($nCaO_2$) produced from flue gas desulfurization (FGD) gypsum, Environ. Technol. Innov., 24 (2021) 101861, doi: 10.1016/j.eti.2021.101861.
[33] Y.Y. Jiang, Z.W. Chen, M.M. Li, Q.H. Xiang, X.X. Wang, H.F. Miao, W.Q. Ruan, Degradation of diclofenac sodium using Fenton-like technology based on nano-calcium peroxide, Sci. Total Environ., 773 (2021) 144801, doi: 10.1016/j.scitotenv.2020.144801.
[34] L. Xiang, Z. Xie, H. Guo, J. Song, D. Li, Y. Wang, S. Pan, S. Lin, Z. Li, J. Han, W. Qiao, Efficient removal of emerging contaminant sulfamethoxazole in water by ozone coupled with calcium peroxide: mechanism and toxicity assessment, Chemosphere, 283 (2021) 131156, doi: 10.1016/j.chemosphere.2021.131156.
[35] P. Yue, S. Hanrui, Z. Yitong, V.M. Hamed, L. Mingce, CaO_2 based Fenton-like reaction at neutral pH: Accelerated reduction of ferric species and production of superoxide radicals, Water Res., 145 (2018) 731–740.
[36] Z. Ming, D.D. Kevin, P. Minkyu, B.N. Alec, C.C. Erica, L. Yongmei, A.S. Shane, Attenuation of pharmaceutically active compounds in aqueous solution by UV/CaO_2 process: influencing factors, degradation mechanism and pathways, Water Res., 164 (2019) 114922, doi: 10.1016/j.watres.2019.114922.
[37] S. Hashemian, Fenton-like oxidation of Malachite green solutions: kinetic and thermodynamic study, J. Chem., 2013 (2013) 809318, doi: 10.1155/2013/809318.
[38] E. Kulaksız, B. Kayan, B. Gözmen, D. Kalderis, N. Oturan, M.A. Oturan, Comparative degradation of 5-fluorouracil in aqueous solution by using H_2O_2-modified subcritical water, photocatalytic oxidation and electro-Fenton processes, Environ. Res., 204 (2022) 111898, doi: 10.1016/j.envres.2021.111898.
[39] N.T. Dung, N.T. Hoa, V.D. Thao, N.N. Huy, A comprehensive study on the heterogeneous electro-Fenton degradation of tartrazine in water using $CoFe_2O_4$/carbon felt cathode, Chemosphere, 287 (2022) 132141, doi: 10.1016/j.chemosphere.2021.132141.
[40] H. Xu, H. Guo, C. Chai, N. Li, X. Lin, W. Xu, Anodized graphite felt as an efficient cathode for in-situ hydrogen peroxide production and Electro-Fenton degradation of Rhodamine B, Chemosphere, 286 (2022b) 131936, doi: 10.1016/j.chemosphere.2021.131936.
[41] S.N.G. Eroi, A.S. Ello, D. Diabaté, D.B. Ossonon, Heterogeneous WO_3/H_2O_2 system for degradation of Indigo Carmin dye from aqueous solution, S. Afr. J. Chem. Eng., 37 (2021) 53–60.
[42] O.M. Cornejo, M. Ortiz, Z.G. Aguilar, J.L. Nava, Degradation of Acid violet 19 textile dye by electro-peroxone in a laboratory flow plant, Chemosphere, 271 (2021) 129804, doi: 10.1016/j.chemosphere.2021.129804.
[43] F. Anjum, A.M. Asiri, M.A. Khan, M.I. Khan, S.B. Khan, K. Akhtar, E.M. Bakhsha, K.A. Alamry, S.Y. Alfifi, S. Chakraborty, Photo-degradation, thermodynamic and kinetic study of carcinogenic dyes via zinc oxide/graphene oxide nanocomposites, J. Mater. Res. Technol., 15 (2021) 3171–3191.
[44] S. Ali, S. Basak, S. Sikdar, M. Roy, Synergetic effects of green synthesized CeO_2 nanorod-like catalyst for degradation of organic pollutants to reduce water pollution, Environ. Nanotechnol. Monit. Manage., 16 (2021) 100539, doi: 10.1016/j.enmm.2021.100539.
[45] M. Saxena, R. Saxena, Fast and efficient single step synthesis of modified magnetic nanocatalyst for catalytic reduction of 4-nitrophenol, Mater. Chem. Phys., 276 (2021) 125437, doi: 10.1016/j.matchemphys.2021.125437.
[46] R. Jain, S. Mendiratta, L. Kumar, A. Srivastava, Green synthesis of iron nanoparticles using *Artocarpus heterophyllus* peel extract and their application as a heterogeneous Fenton-like catalyst for the degradation of Fuchsin Basic dye, Curr. Res. Green Sustainable Chem., 4 (2021) 100086, doi: 10.1016/j.crgsc.2021.100086.
[47] N.S. Freitas, M. Alzamora, D.R. Sanchez, Y.E. Licea, J.D. Senra, N.M. Carvalho, Green palladium nanoparticles prepared with glycerol and supported on maghemite for dye removal application, J. Environ. Chem. Eng., 9 (2021) 104856, doi: 10.1016/j.jece.2020.104856.
[48] D.S. Duc, Response surface optimization for decolorization of Basic blue 41 by Fenton's reagent, Int. J. Chemtech. Res., 6 (2014) 3943–3948.
[49] D. Solomon, Z. Kiflie, S.V. Hulle, Using Box–Behnken experimental design to optimize the degradation of Basic blue 41 dye by Fenton reaction, Int. J. Ind. Chem., 11 (2020) 43–53.
[50] N.M. Mahmoodi, J. Abdi, Nanoporous metal-organic framework (MOF-199): synthesis, characterization and photocatalytic degradation of Basic blue 41, Microchem. J., 144 (2019) 436–442.
[51] E. Stathatos, D. Papoulis, C.A. Aggelopoulos, D. Panagiotaras, A. Nikolopoulou, TiO_2/palygorskite composite nanocrystalline films prepared by surfactant templating route: synergistic effect to the photocatalytic degradation of an azo-dye in water, J. Hazard. Mater., 211 (2012) 68–76.
[52] Y. Jiang, Y. Sun, H. Liu, F. Zhu, H. Yin, Solar photocatalytic decolorization of CI Basic blue 41 in an aqueous suspension of TiO_2–ZnO, Dyes Pigm., 78 (2008) 77–83.
[53] Y. Benrighi, N. Nasrallah, T. Chaabane, V. Sivasankar, A. Darchen, O. Baaloudj, Characterization of $CoCr_2O_4$ semiconductor: a prominent photocatalyst in the degradation of Basic blue 41 from wastewater, Opt. Mater., 122 (2021) 111819, doi: 10.1016/j.optmat.2021.111819.

[54] T.E. Kweinor, E. Obotey Ezugbe, D. Asante-Sackey, E.K. Armah, S. Rathilal, Response surface methodology: photocatalytic degradation kinetics of Basic blue 41 dye using activated carbon with TiO_2, Molecules, 26 (2021) 1068, doi: 10.3390/molecules26041068.
[55] S. Mohammadi-Aghdam, M.E. Olya, Degradation of CI Basic blue 41 using modified TiO_2 nanocomposite in a rectangular semibatch photoreactor, Prog. Color Color. Coat., 8 (2014) 47–57.
[56] L. Nouri, S. Hemidouche, A. Boudjemaa, F. Kaouah, Z. Sadaoui, K. Bachari, Elaboration and characterization of photobiocomposite beads, based on titanium(IV) oxide and sodium alginate biopolymer, for Basic blue 41 adsorption/photocatalytic degradation, Int. J. Biol. Macromol., 151 (2020) 66–84.
[57] W.R. Kartiko, I. Suciani, E. Savitri, R. Reynaldi, A. Budhyantoro, Photocatalytic decolorization of Basic blue 41 using TiO_2-Fe_3O_4-bentonite coating applied to ceramic in continuous system, Chem. Eng. Commun., 207 (2020) 203–212.
[58] A. Rapsomanikis, D. Papoulis, D. Panagiotaras, E. Kaplani, E. Stathatos, Nanocrystalline TiO_2 and halloysite clay mineral composite films prepared by sol-gel method: synergistic effect and the case of silver modification to the photocatalytic degradation of Basic blue-41 azo dye in water, Global Nest J., 16 (2014) 485–498.
[59] A. Sadeghzadeh-Attar, Binary Zn-doped SnO_2/Al_2O_3 nanotube composites for visible-light-driven photocatalytic degradation of Basic blue 41, ACS Appl. Nano Mater., 3 (2020) 9931–9942.
[60] M. Behpour, P. Shirazi, M. Rahbar, Immobilization of the Fe_2O_3/TiO_2 photocatalyst on carbon fiber cloth for the degradation of a textile dye under visible light irradiation, React. Kinet. Mech. Catal., 127 (2019) 1073–1085.
[61] M.A. Shaida, A.K. Sen, R.K. Dutta, Alternate use of sulphur rich coals as solar photo-Fenton agent for degradation of toxic azo dyes, J. Cleaner Prod., 195 (2018) 1003–1014.
[62] N.M. Mahmoodi, S. Keshavarzi, M. Ghezelbash, Synthesis of nanoparticle and modelling of its photocatalytic dye degradation ability from colored wastewater, J. Environ. Chem. Eng., 5 (2017) 3684–3689.
[63] H. Kenfoud, N. Nasrallah, D. Meziani, M. Trari, Photoelectrochemical study of the spinel $CaFe_2O_4$ nanostructure: application to Basic blue 41 oxidation under solar light, J. Solid State Electrochem., 25 (2021) 1815–1823.
[64] M. Abbasi, N.R. Asl, Sonochemical degradation of Basic blue 41 dye assisted by nanoTiO_2 and H_2O_2, J. Hazard. Mater., 153 (2008) 942–947.
[65] J. Parsa, M. Abbasi, Modeling and optimizing of sonochemical degradation of Basic blue 41 via response surface methodology, Open Chem., 8 (2010) 1069–1077.
[66] N. Wang, T. Zheng, G. Zhang, P. Wang, A review on Fenton-like processes for organic wastewater treatment, J. Environ. Chem. Eng., 4 (2016) 762–787.
[67] A. Babuponnusami, K. Muthukumar. A review on Fenton and improvements to the Fenton process for wastewater treatment, J. Environ. Chem. Eng., 2 (2014) 557–572.
[68] M. Antonopoulou, C. Kosma, T. Albanis, I. Konstantinou, An overview of homogeneous and heterogeneous photocatalysis applications for the removal of pharmaceutical compounds from real or synthetic hospital wastewaters under lab or pilot scale, Sci. Total Environ., 765 (2021) 144163, doi: 10.1016/j.scitotenv.2020.144163.
[69] M. Pawar, T.S. Sendoğdular, P. Gouma, A brief overview of TiO_2 photocatalyst for organic dye remediation: case study of reaction mechanisms involved in Ce-TiO_2 photocatalysts system, J. Nanomater., 2018 (2018) 5953609, doi: 10.1155/2018/5953609.
[70] D. Wang, M.A. Mueses, J.A.C. Márquez, F. Machuca-Martínez, I. Grčić, R.P.M. Moreira, G.L. Puma, Engineering and modeling perspectives on photocatalytic reactors for water treatment, Water Res., 202 (2021) 117421, doi: 10.1016/j.watres.2021.117421.
[71] L. Andronic, A. Vladescu, A. Enesca, Synthesis, characterisation, photocatalytic activity, and aquatic toxicity evaluation of TiO_2 nanoparticles, Nanomaterials, 11 (2021) 3197, doi: 10.3390/nano11123197.
[72] J.A Coral, C.L. Kitchens, J.L. Brumaghim, S.J. Klaine, Correlating quantitative measurements of radical production by photocatalytic TiO_2 with *Daphnia magna* toxicity, Environ. Toxicol. Chem., 40 (2021) 1322–1334.
[73] J.K. Seol, M. Park, J.M. Im, H.S. Seo, H.J. Park, S.S. Nah, Acute toxicity assessment for TiO_2 photocatalyst (GST) made from wastewater using $TiCl_4$ in rat, Environ. Anal. Health Toxicol., 36 (2021), doi: 10.5620/eaht.2021019.
[74] R. Naima, M. Imen, J. Mustapha, H. Abdelmalek, K. Kamel, M. Sakly, A. Amara, Acute titanium dioxide nanoparticles exposure impaired spatial cognitive performance through neurotoxic and oxidative mechanisms in Wistar rats, Biomarkers, 26 (2021) 760–769.
[75] Y. Fang, M. Dai, W. Ye, F. Li, H. Sun, J. Wei, B. Li, Damaging effects of TiO_2 nanoparticles on the ovarian cells of *Bombyx mori*, Biol. Trace Elem. Res., 200 (2022) 1883–1891.
[76] J. Canlan, Y. Ying, Z. Lei, L. Dan, L. Lingli, Y. Xiaoxue, C. Tianming, Degradation of atrazine, simazine and ametryn in an arable soil using thermal-activated persulfate oxidation process: optimization, kinetics, and degradation pathway, J. Hazard. Mater., 400 (2020) 123201, doi: 10.1016/j.jhazmat.2020.123201.